Multitemporal Surface Deformation Analysis of Amyntaio Slide (Greece) using Remotely Piloted Airborne System and Structure-from-Motion photogrammetry

Emmanuel Vassilakis[1], Michael Foumelis[2], Athanasia Erkeki[3], Evelina Kotsi[4], Issaak Parcharidis[5], Efthymios Lekkas[6]

[1] Remote Sensing Laboratory, Faculty of Geology & Geo-environment, NKUA, Panepistimiopolis Zographou, Greece, (evasilak@geol.uoa.gr)

[2] Geophysical Imaging and Remote Sensing Unit (DRP-IGT), BRGM - French Geological Survey, Orleans, France, (m.foumelis@brgm.fr)

[3] Remote Sensing Laboratory, Faculty of Geology & Geo-environment, NKUA, Panepistimiopolis Zographou, Greece, (aerkeki@geol.uoa.gr)

[4] Natural Hazards Laboratory, Faculty of Geology & Geo-environment, NKUA, Panepistimiopolis Zographou, Greece, (ekotsi@geol.uoa.gr)

[5] Dpt of Geography, Harokopio University, 70 Eleftheriou Venizelou, Kallithea, Greece, (parchar@hua.gr)

[6] Natural Hazards Laboratory, Faculty of Geology & Geo-environment, NKUA, Panepistimiopolis Zographou, Greece, (elekkas@geol.uoa.gr)

Key words: *Amyntaio landslide*; *ground deformation*; *Remotely Piloted Airborne System; photogrammetry*

ABSTRACT

The results of Structure-from-Motion photogrammetry for the quantification of the ground surface deformation due to the massive landslide that occurred at the lignite open pit in Amyntaio, Greece on 10th June 2017, is presented in this paper. This unexpected slide damaged the entire westernmost marginal area of the pit, significant number of buildings and infrastructures (incl. road network, powerlines, biological treatment, houses etc.) of the nearby village of Anargiri, as well as agricultural land at the head of the landslide. We generated a very high-resolution surface topography and corresponding co-registered ortho-rectified images covering a total area of 2 km^2 by analyzing images acquired from Remotely Piloted Airborne Systems (RPASs). A high resolution (0.13 m) Digital Surface Model (DSM) was produced after photogrammetric processing, serving as a reference dataset for comparison with other surveys realized on December 2017 and September 2018. We compared the high-resolution DSMs acquired during the post landslide periods, quantified the overall ground deformation and finally delineated regions of potential risk.

I. INTRODUCTION

The number of published studies that describe possible applications of Unmanned Aerial System (UAS) for the management of natural hazards consequences and the identification or quantification of occurred damages have been strongly increased in the last decade (Giordan *et al.,* 2018).

The use of the mini and micro UASs is practical for small areas and optimal for landslides that often cover an area that ranges from less than one square kilometers up to few square kilometers. High-resolution images acquired by UASs may support the definition of not only the identification of studied landslide limit but also the identification and mapping of the main geomorphological features (Fiorucci *et al.,* 2018). Furthermore, a sequence of low-cost UAS acquisitions over time can provide useful support for the delineation of the surface structures and generally for the study of gravitational process evolution (Niethammer *et al.,* 2012; Liu *et al.,* 2015).

In our application, several UAS field surveys were conducted for the acquisition of aerial images covering a total area of 2 km^2. Three surveys took place at the edge of a massive landslide, which occurred at an open lignite pit in Amyntaio, Greece on 10th June 2017. This phenomenon destroyed the westernmost marginal area of the open pit, as well as significant infrastructure of the nearby village of Anargiri (road network, powerlines, biological treatment, houses), not to mention the agricultural land at the head of the landslide. Several ground displacements are still visible around the village and all the field observation lead to the conclusion that they are still active and ongoing deformation is happening for at least 15 months after the landslide event. In many cases the scarp exceeds one meter size, causing serious destructions at the building structure, especially at the eastern part of Anargiri village (Figure 1).

II. Stratigraphy and Structural Geology

The Amyntaio open pit is located at the NW margin of the Ptolemais basin, which is an elongated structure trending NW-SE. The basin is filled with Late Miocene–Pleistocene lacustrine sediments which in a few places exceed the thickness of 500 meters, which cover metamorphic basement rocks. The entire succession includes intercalations of lignites, lacustrine marl beds, fluvial sands and silts, along with volcanic ash beds covered by alluvial deposits (Anastopoulos & Koukouzas, 1972; Steenbrink *et al.,* 1999).

Several generations of faults are offsetting the lacustrine beds causing displacements that reach even 50 meters of throw (Delongos *et al.,* 2016). They strike NW-SE and NE-SW and they follow the main trending of the two extensional episodes of Late Miocene (NE-SW) and Quaternary (NW-SE), respectively (Pavlides & Mountrakis, 1987; Mercier *et al.,* 1989).

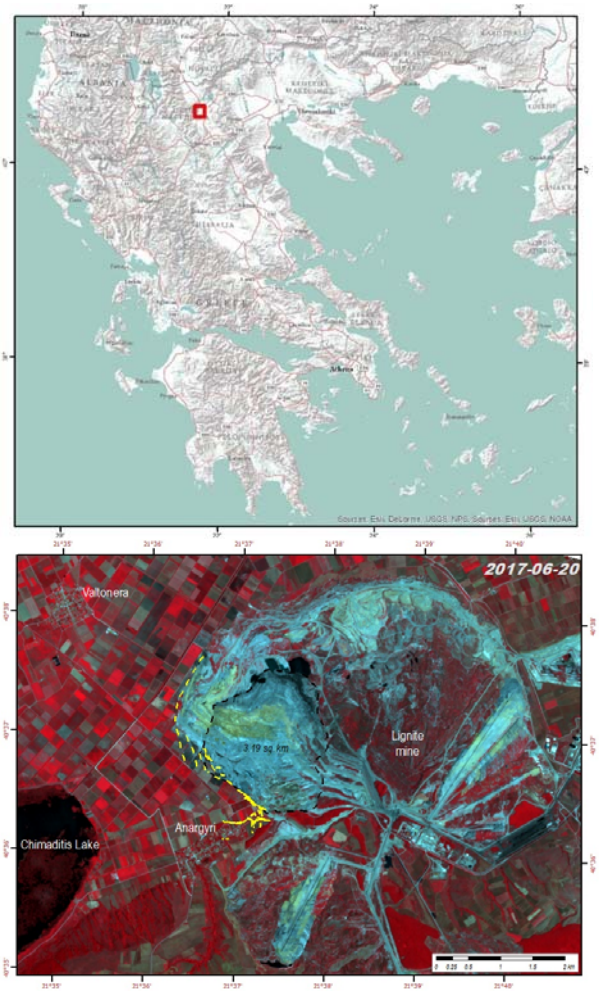

Figure 1. Index map of the Amyntaio open pit location in continental Greece (at the top). At the bottom a false colour RapidEye satellite image acquired ten days after the landslide showing the entire lignite open mine. The black dashed line surrounds the landslide debris, whereas the yellow ones show the surface fractures mapped after the occurrence of the slide phenomenon.

III. Data and Methodology

The aim of this multitemporal study was to create a series of Digital Surface Models (DSMs) along with the ortho-photo-mosaics of the same area, based on the Structure-from-Motion photogrammetry (Westoby *et al.,* 2012; Granshaw, 2018). Hundreds of aerial images are acquired during each flight and they are combined through photogrammetric software to produce accurate micro-topography and high-resolution imagery.

The open surface of the area of interest was extracted with the implementation of a rotor-wing UAS (DJI Phantom 4 Advanced drone) during the field surveys. It was used to collect high-resolution natural colour images with its built-in camera (with 3.61 mm focal length) bundled on a two-axis gimbal.

Each survey was completed after five -flights, each of them lasting 15 minutes, which covered a 2 km^2 selected area that included the Anargiri village as well as the edge of the landslide. The flights were programmed at a flight elevation of 140 m above three different take off points and the overlap was set at 75% along the flight line and 65% at the sides of the flights (Pepe *et al.,* 2018). During the programming of the image acquisition, the flight height and the density of the images had to be taken under serious consideration, in terms of the battery usage limitations. The percentage of overlapping is quite crucial as it had to be high enough for a successive photogrammetric processing and ortho-photo-mosaic construction without any artefacts. The UAS platform is equipped with a GNSS antenna which provides quite good precision especially for the horizontal positions of which may help the alignment of the images captured during the survey (Fonstad *et al.,* 2013). Despite this we used 8 ground control points (GCPs) measured with high precision Real Time Kinematics Geodetic Navigation Satellite System (RTK-GNSS) to maximize the accuracy of the products, since a comparative study was the main objective (Fugazza *et al.,* 2018).

The first survey was conducted about three months after the landslide during September 2017. A total of 257 images (4000 x 3000 pixels each) was acquired with sufficient front and side overlaps. The same overlaps were used for the second field survey (December 2017, 322 images) and the third survey (September 2018, 401 images), with reducing the flight elevation from 140 m to 120 m above ground to increase the spatial resolution of the outcome DSMs and mosaics.

The procedure started with aligning the aerial images and creating a sparse 3D point cloud followed by a mesh generation. Locating the GCPs on every image and inserting the exact coordinates and elevation measured by the RTK-GNSS was the next step in the methodology, which is the recommended photogrammetric procedure outlined by Agisoft (2016) and was slightly modified for reducing geometry errors and constructing a dense point cloud. Three of them were constructed

consisted of about 800,000 points for each one of the three surveys.

The information for each point of them includes values of reflectance at the visible (BGR) spectra along with X, Y, Z coordinates, which were calculated after taking into account the positions of the camera when shooting at each point from different angles (Westoby et al 2012). The procedure continued with meshing the original images as fine topographic details were available. Texturing was also applied to the resulted mesh in a later step and an ortho-image was generated as well as a DSM (Mancini *et al.,* 2013) (Figure 2).

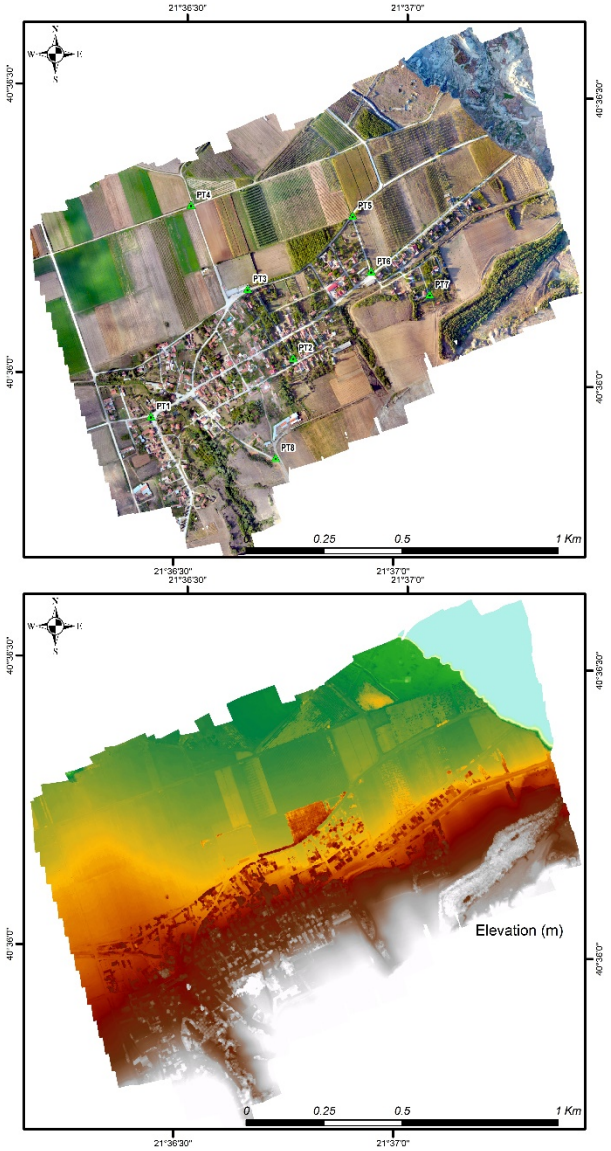

Figure 2. The earliest (September 2017) ortho-photo-mosaic of the area of interest (top) along with the GCPs locations and the DSM of the same period (bottom).

The final spatial resolution of the three ortho-images is calculated at 6-10 cm and the DSMs' pixel size is at 10-13 cm, depending on the flight elevation and the density of the overlapping images. The feature density of the point clouds is given by the generated reports at 60-95 points/m^2 respectively. At all three processing periods the error is less than the dimensions of a pixel (0.7-0.6 pix) and it is worth to mention that the z-error at the GCPs' location, after the completion of the processing, never exceeded 1 cm.

IV. Results

The multitemporal study of the deformations at the area surrounding the upper part of the landslide was based on three DSMs that were created during a year of observations (September 2017 – September 2018). The height elevation changes at the area around the Anargiri village were measured with high detail and accuracy and were also verified by the RTK measurement of the GCPs that were established throughout the area of interest.

The village is developed along a NE-SW elongated shape whereas its NE edge was affected by the collapse in the open mine. Most of the residential area was stable after the landslide event but the NE part seems to be under continuous and severe deformation even after 1.5 year after the failure happened.

Several surface fractures have appeared around the wider area of the village either on the road network or in the cultivated parcels (Figure 3).

Figure 3. The main E-W trending surface fracture immediately after the landslide (top) and fifteen months later (bottom). It is clear that the fracture is still active and the displacement exceeds 0.7 meters.

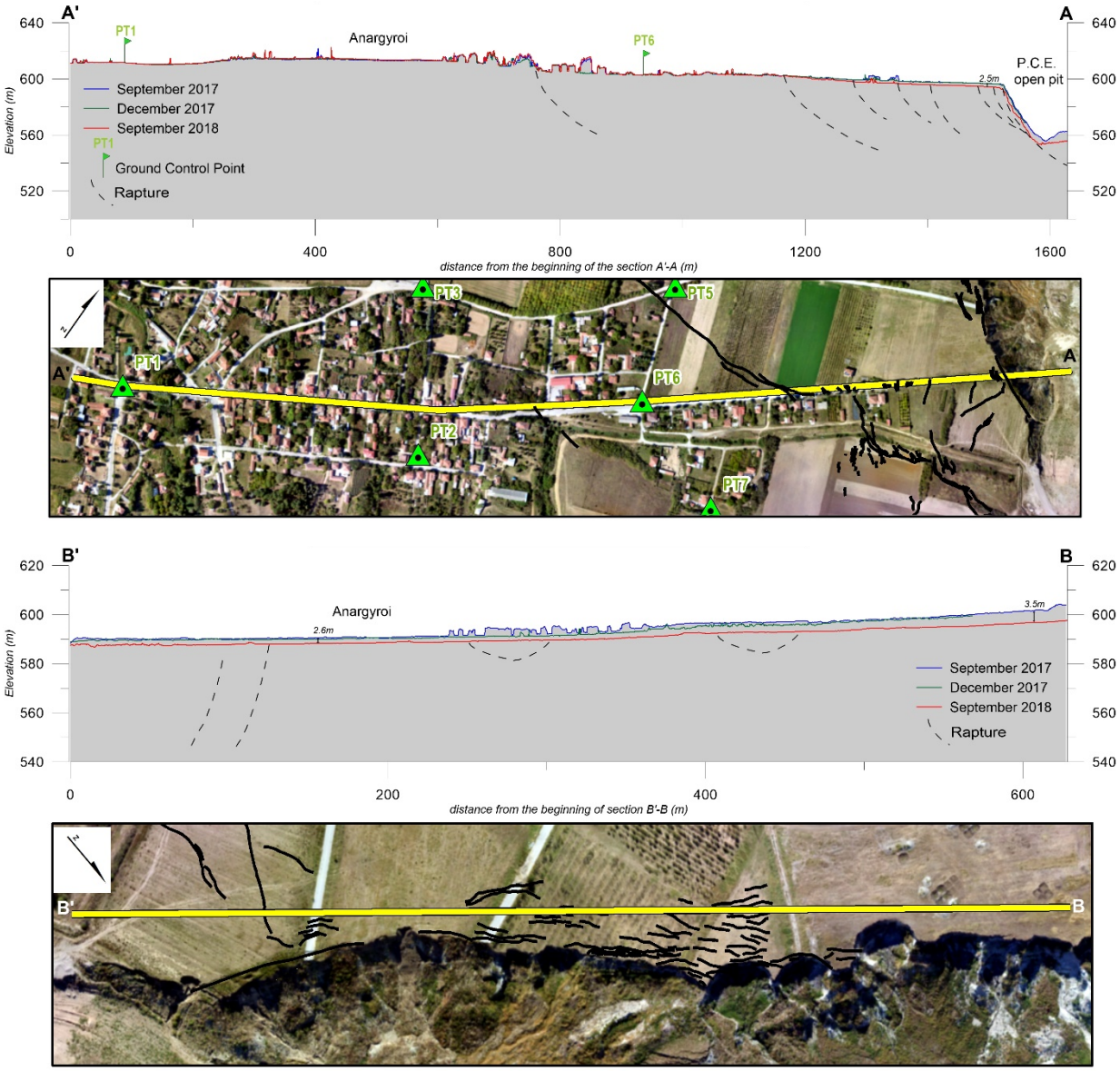

Figure 4. Two cross-sections with normal trending showing the change of the topography across the crown of the landslide (top) and along the cliff created after the event (bottom). The resulted elevation profiles after the three UAS flights are represented with different colors at the sections. The continuous black lines represent the surface fractures as mapped on the ground and the dashed ones represent their hypothetic underground projection. The green triangles and flags show the GCPs' locations.

A large number of buildings were also affected by these fractures causing the residents to move to safer living places. It is more than apparent that the fractures are still active since the displacement along the main structures increases and is visible even without special equipment.

It was very important to find a way to quantify the rate of every displacement and it seems that one of the most promising methodologies include the comparison of the Structure-from-Motion photogrammetry outcomes (Fonstad *et al.,* 2013). After the three UAS campaigns it became feasible to create elevation grids with high accuracy and precision. The next step was to locate the areas where the measured elevation was different revealing surface deformation during the post-landslide period.

The multi-temporal high-resolution ortho-photo images proved to be very helpful in mapping the surface fractures. It was quite clear that this methodology provides useful tools for digitizing on screen in very large scales as the cracks on the ground or at the houses of the residential areas can be very obvious since the image resolution allows a precise interpretation of fractures' size and locations.

Several fracture trending at different orientations were mapped on a GIS platform but two were the dominant ones. The first cross-section trending E-W shows the largest displacement throw and seems to influence all kinds of land uses (residential, roads, agricultural).

The second cross-section trending parallel to the landslide scarp (SE-NW) is clearly related to the collapse

orientation pointing to the discontinuities that are most prominent to be activated in the immediate next phase.

The comparison of the three DSMs showed that between September 2017 and December 2017, not much deformation was recorded. The entire area seemed to be quite stable and the height values at most of the points of the point clouds were rather identical or changed at centimeter order. That happened when the ground consisted of non-vegetated soil or concrete, since the cultivated or forested areas covered by vegetation that changed in the three-month period gave significant different elevation values.

This was also in agreement with the GCP measurements, which were based on the asphalt and no elevation change was observed.

On the contrary, the comparison between the DSMs of September 2017 and September 2018 showed significant change at the elevation values at the NE part of the area of interest. Even though, most of the GCPs were more or less stable, with minimum changes and compatible with the errors given by the specifications of the equipment, the large area neighboring the landslide crown showed significant deformation. The maximum DSM differences were located at the areas that have collapsed after the major event. These were much smaller cases of collapse material coming from the edge of the crown and end up into the open mine area. The elevation difference values at those cases exceeded the 50 meters as this was the fresh prone height, which was revealed after the failure.

The SW part of the Anargiri village, which lies about a kilometer away from the landslide crown seems to be stable even after a year from the first campaign and it is quite certain that if the conditions remain the same the safety of the residents could be guaranteed.

The safety zone ends at the middle of the village development between GCPs PT2 and PT6 (Figure 4), where the SW-most surface fracture was mapped. This is the western margin of the deformation area which is rather obvious with bare eyes more to the east, where the landslide crown is located. Two cross sections (Figure 4) were constructed based on the DSMs' elevations with normal orientations.

The first one (1,600 meters long) follows the main village road from the stable area (SW) to the landslide (NE) passing through the GCPs PT1 and PT6 for control reasons and crossing the mapped surface fractures. The elevation difference values seem to increase at the area between PT6 and the landslide crown reaching the value of 2.6 m just before the recently formed prone, which was revealed after the June 2017 landslide. The cross section shows the hypothetical prolongation of the fractures towards the subsurface, based on their dimensions and orientation.

The second one (about 600 meters long) is located almost parallel to the landslide main scarp. It also trends oblique to most of the mapped fractures and the elevation difference values between the first and the last campaign exceeds the 3.5 m with gradually increasing values from SE to NW (Figure 4).

V. Conclusions

The described methodology introduces a simple but very convenient way of combining datasets containing elevation information throughout a given time period, in order to quantify the displacement rate and consequently the surface deformation.

Even though the data collection through the UAS campaigns proved to be quite difficult and dangerous for the humans and the equipment, as several parameters had to be taken under consideration, such as the weather conditions, the continuous development of the phenomenon, the failure of different kinds of equipment to work together etc.

Additionally, large amounts of data regarding the highest resolution that could be achieved, should be processed demanding lots of resources and long waiting times to provide accurate results. The comparison between the different time periods requires long processing times as well as several software packages within Geographic Information System platform and finally determine and quantify the location and the amount of deformation.

The order of the surface deformation exceeds the 3 m of subsidence along the crown of the landslide at the margins of the Amyntaio open pit, as measured after comparing the DSMs of the three time periods. The crown trace seems to move towards the village and getting quite dangerous for the farmers as it is very well imprinted by the constructed multitemporal ortho-photo-mosaics.

By employing the methodology described above, we collected, processed and analyzed contemporary aerial images acquired by a low cost UAS covering a time period of one year.

The deformation rate that we calculated were not homogeneous along the entire area of interest but the methodology provided useful information for the elevation difference and the trend of the subsidence, which will probably lead to another episode of the expansion of the landslide.

Specifically, the deformation values exceeded the 3.5 m delineating a wedge type subsidence with increasing difference values from the residential area towards the unstable landslide area.

It is more than clear that these campaigns and the multitemporal data processing depict the risk at specific locations, despite the fact that several kinds of protection measures have been taken or are planned to be implemented in the near future by the authorities, as the residents' safety should be the first priority and setting up an early-warning system could be very useful.

References

Agisoft, (2016). Agisoft Photoscan user manual: professional edition (v.1.2), Retrieved 23/7/2016, http://www.agisoft.com/pdf/photoscan-pro_1_2_en.pdf.

Anastopoulos, J. and Koukouzas, N. (1972). Economic Geology of the Southern Part Ptolemais Lignite Basin (Macedonia – Greece). Geological & Geophysical Research, IGME, Athens.

Delogkos, E., Manzocchi, T., Childs, C., Sachanidis, C., Barbas, T., Scheopfer, P.J.M., Chatzipetros, A., Pavlides, S. and Walsh, J.J. (2016). Throw partitioning across normal fault zones in the Ptolemais Basin, Greece. In: Childs, C., Holdsworth, R.E., Jackson, C.A.-L., Manzocchi, T., Walsh, J.J., Yielding, G. (Eds.), Geometry and Growth of Normal Faults, vol. 439. Special Publications Geological Society, London.

Fiorucci, F., Giordan, D., Santangelo, M., Dutto, F., Rossi, M., and Guzzetti, F. (2018). Criteria for the optimal selection of remote sensing optical images to map event landslides, Nat. Hazards Earth Syst. Sci., 18, pp. 405–417.

Fonstad, M., Dietrich, J., Courville, B., Jensen, J., Carbonneau, P. (2013). Topographic structure from motion: a new development in photogrammetric measurement. Earth Surface Processes and Landforms, 38, pp. 421-430.

Fugazza, D., Scaioni, M., Corti, M., D'Agata, C., Azzoni, R.S., Cernuschi, M., Smiraglia, C., Diolaiuti, G.A. (2018). Combination of UAV and terrestrial photogrammetry to assess rapid glacier evolution and map glacier hazards. Nat. Hazards Earth Syst. Sci., 18, pp. 1055-1071.

Giordan, D., Hayakawa, Y., Nex, F., Remondino, F., and Tarolli, P. (2018). Review article: the use of remotely piloted aircraft systems (RPASs) for natural hazards monitoring and management, Nat. Hazards Earth Syst. Sci., 18, pp. 1079-1096.

Granshaw, S.I., (2018). Structure from motion: origins and originality. The Photogrammetric Record, 33, pp. 6-10.

Liu, C.C., Chen, P.L., Tomoya, M., and Chen, C.Y. (2015). Rapidly responding to landslides and debris flow events using a lowcost unmanned aerial vehicle, J. Remote Sens. 9, pp. 1–11

Mancini, F., Dubbini, M., Gattelli, M., Stecchi, F., Fabbri, S., Gabbianelli, G. (2013). Using Unmanned Aerial Vehicles (UAV) for High-Resolution Reconstruction of Topography: The Structure from Motion Approach on Coastal Environments. Remote Sensing, 5, 6880.

Mercier, J.L., Sorel, D., Vergely, P. & Simeakis, K. (1989). Extensional tectonic regimes in the Aegean basins during the Cenozoic. Basin Research, 2, pp. 49–71.

Niethammer, U., James, M. R., Rothmund, S., Travelletti, J., and Joswig, M. (2012). UAV-based remote sensing of the Super-Sauze landslide: evaluation and results, Eng. Geol., 128, pp. 2–11.

Pavlides, S. and Mountrakis, D. (1987). Extensional tectonics of northwestern Macedonia, Greece, since the late Miocene. Journal of Structural Geology, 9, pp. 385–392.

Pepe, M., Fregonese, L., Scaioni, M. (2018). Planning airborne photogrammetry and remote-sensing missions with modern platforms and sensors. European Journal of Remote Sensing, 51, pp. 412-436.

Steenbrink, J., vanVugt,N., Hilgen, F.J., Wijbrans, J.R. and Meulenkamp, J.E. (1999). Sedimentary cycles and volcanic ash beds in the Lower Pliocene lacustrine succession of Ptolemais (NW Greece): discrepancy between $^{40}Ar/^{39}Ar$ and astronomical ages. Palaeogeography, Palaeoclimatology, Palaeoecology, 152, pp. 283–303.

Westoby, M.J., Brasington, J., Glasser, N.F., Hambrey, M.J., Reynolds, J.M. (2012). 'Structure-from-Motion' photogrammetry: A low-cost, effective tool for geoscience applications. Geomorphology, 179, pp. 300-314.